



## Research paper

A novel 3DOM Ti<sup>3+</sup> self-doped TiO<sub>2</sub> for photocatalytic removal of NODong Wang<sup>a</sup>, Siyuan Zheng<sup>a,b</sup>, Jie Yao<sup>b</sup>, Yawen Wang<sup>a,\*</sup>, Yu Huang<sup>b,\*</sup>, Caimei Fan<sup>a</sup>, Wei Huang<sup>a</sup><sup>a</sup> College of Chemistry and Chemical Engineering, Taiyuan University of Technology, Taiyuan 030024, China<sup>b</sup> Key Lab of Aerosol Chemistry & Physics, Institute of Earth Environment, Chinese Academy of Sciences, Xi'an 710075, China

## HIGHLIGHTS

- A 3DOM Ti<sup>3+</sup> self-doped TiO<sub>2</sub> is synthesized by a facile sol-gel template and ice-water quenching method.
- The 3DOM Ti<sup>3+</sup> Self-doped TiO<sub>2</sub> display superior photocatalytic activity on removing of NO under visible light irradiation.
- The Ti<sup>3+</sup> self-doping and slow photon effect of 3DOM structure act as dual-function for charge separation and efficient light harvesting in photocatalysis.

## ARTICLE INFO

**Keywords:**  
Self-doped TiO<sub>2</sub>  
3DOM  
NO removal  
Porous materials  
XPS

## ABSTRACT

A novel three dimensionally ordered macroporous (3DOM) Ti<sup>3+</sup> self-doped TiO<sub>2</sub> with an ordered distribution of macropores in the diameter of 270 nm is synthesized by a facile colloidal polystyrene template sol-gel and ice-water quenching method. The performance of photocatalytic removal of NO from continuous air flow with visible light irradiation show 3DOM Ti<sup>3+</sup> self-doped TiO<sub>2</sub> has enhanced efficiency under visible light irradiation. The improved photocatalytic efficiency could contribute to the presence of Ti<sup>3+</sup> doping induced by ice-water quenching and the 3DOM structure with a large specific surface area.

## 1. Introduction

Titanium dioxide (TiO<sub>2</sub>) is one of promising photocatalysts in consideration of its cheapness, non-toxicity, and outstanding photochemical stability. However, the drawbacks, weak light adsorption in visible-light region and high recombination of photogenerated electron-hole, largely restrain its photocatalytic performance [1]. Up to now, there are plenty of methods can improve these drawbacks, like metal loading, metal oxide loading, foreign elements doping, and so on [2]. Besides of that, creating reduced metal ions doping was shown to be better to improve the photocatalytic activity by improving visible-light absorption, narrowing the band gap and reducing carrier recombination [3,4]. A variety of ways have been implemented to dop Ti<sup>3+</sup> in TiO<sub>2</sub>, such as hydrogenation [5], redox with reducing agents [6], photochemical synthesis [7], and so on. And recently, Liu et al. demonstrated ice-water quenching can be used as a general methodology to implant self-dopants in TiO<sub>2</sub> for increasing its photocatalytic activity [8].

Three dimensionally ordered macroporous materials, with the periodic structure, can forbid the propagation of light by the band gap scattering effect, increase the path length of light through slow photon effect and result in a stop-band reflection because of Bragg coherent

diffraction [9]. It is found that the light absorption could be significantly enhanced by 3DOM structure [10]. The 3DOM structure materials can be easily fabricated by simple hard template sol-gel method [11]. Accordingly, a series of 3DOM TiO<sub>2</sub> materials, such as 3DOM TiO<sub>2</sub> [12,13], 3DOM Fe<sup>3+</sup>-TiO<sub>2</sub> [14] and 3DOM TiO<sub>2</sub>-Au-CdS [15], have been prepared and used in dye-sensitized solar cells, H<sub>2</sub> production and degradation applications.

Inspired by the ice-water quenching method for synthesizing Ti<sup>3+</sup> self-doped TiO<sub>2</sub>, we believe a novel Ti<sup>3+</sup> self-doped TiO<sub>2</sub> with three dimensionally ordered structure could be synthesized by only changing the way of cooling during fabricating 3DOM TiO<sub>2</sub> using hard template sol-gel method. Therefore, in the present research, we synthesized 3DOM Ti<sup>3+</sup> self-doped TiO<sub>2</sub> (3DOM-Ti<sup>3+</sup>-TiO<sub>2</sub>) by a facile colloidal polystyrene template sol-gel and ice-water quenching method. The 3DOM-Ti<sup>3+</sup>-TiO<sub>2</sub> shows excellent efficiency on photocatalytic NO removal from continuous air flow under visible light irradiation.

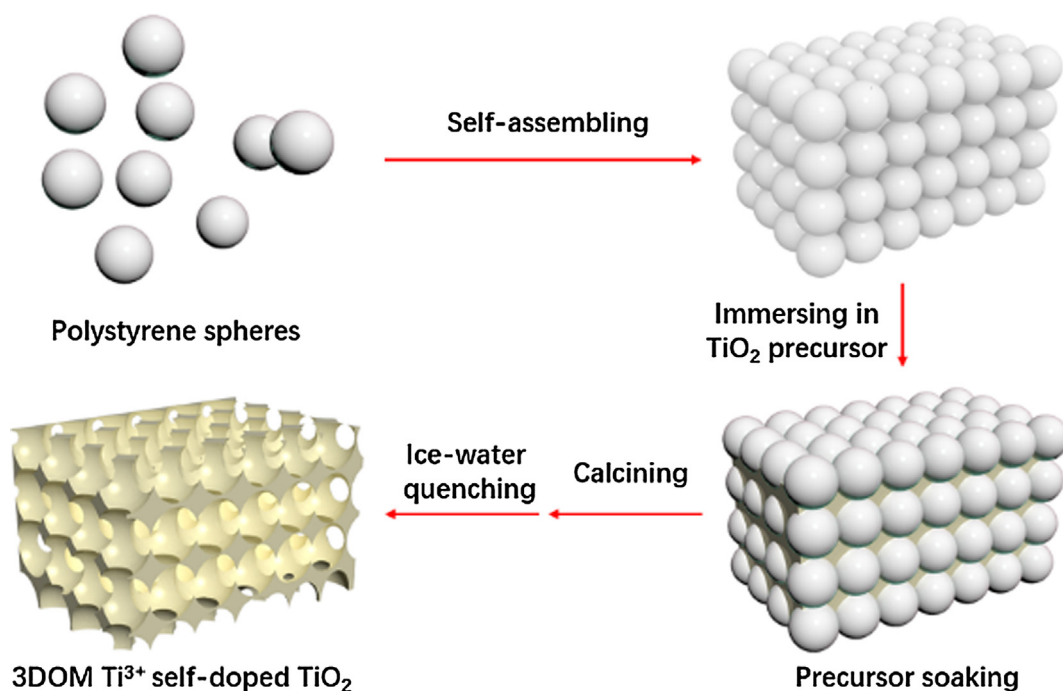
## 2. Experimental section

## 2.1. Preparation of polystyrene (PS) colloidal crystal template

Sodium hydroxide, styrene and potassium persulfate were

\* Corresponding authors.

E-mail addresses: [wangyawen@tyut.edu.cn](mailto:wangyawen@tyut.edu.cn) (Y. Wang), [huangyu@ieecas.cn](mailto:huangyu@ieecas.cn) (Y. Huang).



Scheme 1. Schematic procedure for the preparation of the 3DOM  $\text{Ti}^{3+}$  self-doped  $\text{TiO}_2$ .

purchased from Aldrich. PS template were synthesized by an emulsion polymerization method [16].

## 2.2. Fabrication of 3DOM $\text{Ti}^{3+}$ self-doped $\text{TiO}_2$

3DOM  $\text{Ti}^{3+}$  self-doped  $\text{TiO}_2$ , noted as 3DOM- $\text{Ti}^{3+}$ - $\text{TiO}_2$ , was fabricated as follows (Scheme 1). 0.6 mL hydrochloric acid was dissolved into 60 mL of water. Then 6 mL of tetrabutyl titanate was added dropwise into the solution. The above mixture was stirring at ice bath overnight and aged two weeks to obtain the solution of  $\text{TiO}_2$  precursor. Then 3.5 g PS was immersed into the precursor, filtered and dried at 60 °C in the vacuum drying oven and calcined at 300 °C for 4 h with a rate of 0.5 °C/min in muffle furnace. And then the obtained hot powder was directly thrown into ice-water (ca. 0–4 °C) for rapid quenching. The quenched sample was filtered and then dried at 70 °C for 12 h in the vacuum drying oven for further use. For comparison, the  $\text{Ti}^{3+}$  self-doped  $\text{TiO}_2$ , denoted as  $\text{Ti}^{3+}$ - $\text{TiO}_2$ , was prepared by the same procedure without PS template. And the non-doped  $\text{TiO}_2$ , denoted as  $\text{TiO}_2$ , was prepared by the same procedure without PS template and ice-water quenching.

## 2.3. Photocatalytic degradation of NO

The photocatalytic activity of the as-synthesized samples was investigated through the removal of NO at ppb level in a continuous flow reactor (30 cm × 15 cm × 10 cm) under simulated visible light irradiation at room temperature. The dispersed photocatalyst (0.1 g) was coated on a glass dish (D = 9.0 cm). Then the dishes were treated at 70 °C until complete removal of water in the suspension. The simulated visible light source was a commercial 300 W Xe arc lamp (PLS-SXE 300, Beijing) with a UV cut-off filter ( $\lambda > 420$  nm), which was vertical placed 20 cm above the reactor. The light intensity at the surface of the as synthesized samples was controlled at 0.75 W  $\text{cm}^{-2}$  as measured by a photometer (THORLABS PD130, USA). The NO gas at ppb level was obtained from a compressed gas cylinder at a concentration of 50 ppm of NO ( $\text{N}_2$  balance). The 50 ppm of NO was diluted to about 420 ppb by the air stream from a zero air generator. The flow rate of the gas streams was controlled at 3 L  $\text{min}^{-1}$  by a mass flow controller. The

lamp was not turned on until the adsorption–desorption equilibrium among catalysts, gases and water vapor was obtained. The concentration of NO,  $\text{NO}_2$ , and NOx was continuously measured every 1 min by a NOx analyzer (Ecotech, 9841) at a sampling rate of 0.6 L  $\text{min}^{-1}$ . The removal ratio (R) of NO after irradiation was calculated according to the following equation:

$$R(\%) = (1 \times C/C_0) \times 100\% \quad (1)$$

where C is the outlet concentration of NO each access gases, and  $C_0$  is the inlet concentration before irradiation.

## 2.4. Characterization

The crystal phases of the materials were detected by the X-ray powder diffraction (XRD; SHIMADZU, Lab XRD-6000). XPS characterization was analyzed on ThermoFisher Scientific photoelectron spectrometer (Escalab 250Xi), and the radiation source was Mg K $\alpha$  (1253.6 eV). The C 1s peak (284.6 eV) was used as the standard to rectify the binding energies. The macro-porous structure of the semiconductor was analyzed by the field-emission scanning electron microscope (SEM, JEOL, JSM-6700F). The elemental distribution and inner structure were obtained through transmission electron microscopy (TEM, JEOL, JEM-2100). The Brunauer-Emmett-Teller (BET) surface area of resulted samples were obtained from  $\text{N}_2$  adsorption/desorption isotherms at 77 K (ASAP 2020 automatic analyzer). The samples were degassed at 110 °C prior to analysis. The UV–Vis Diffused Reflectance Spectrum of the resulted samples were performed on a Varian Cary 100 Scan UV–visible system equipped with a labsphere diffuse reflectance accessory in the wavelength range of 200–800 nm. Photoelectrochemical properties of the as-prepared samples were evaluated using a Parstat 4000 electrochemical workstation (USA) in a conventional three-electrode cell, with a platinum plate as the counter electrode and an Ag/AgCl electrode as the reference electrode. The working electrode was prepared by dispersing the 20 mg sample into 4 mL Nafion ethanol solution to obtain homogeneous suspension by using the ultrasonic dispersion method for 30 min. Afterwards, the suspension was coated onto a F-doped tin oxide-conducting glass and dried at room temperature. The photocurrent-time curves were measured at 0.2 V versus Ag/AgCl in 0.5 mol/L  $\text{Na}_2\text{SO}_3$  at ambient

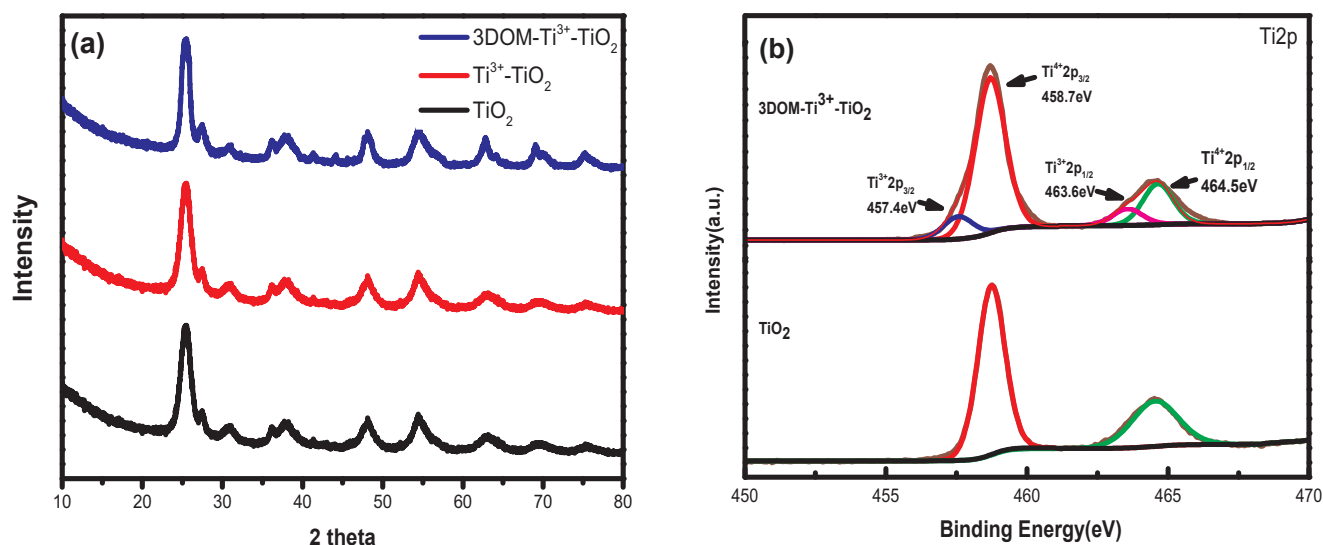


Fig. 1. (a) XRD patterns of the 3DOM-Ti<sup>3+</sup>-TiO<sub>2</sub>, Ti<sup>3+</sup>-TiO<sub>2</sub> and TiO<sub>2</sub>; (b) the Ti2p XPS spectra of the sample 3DOM-Ti<sup>3+</sup>-TiO<sub>2</sub> and TiO<sub>2</sub>.

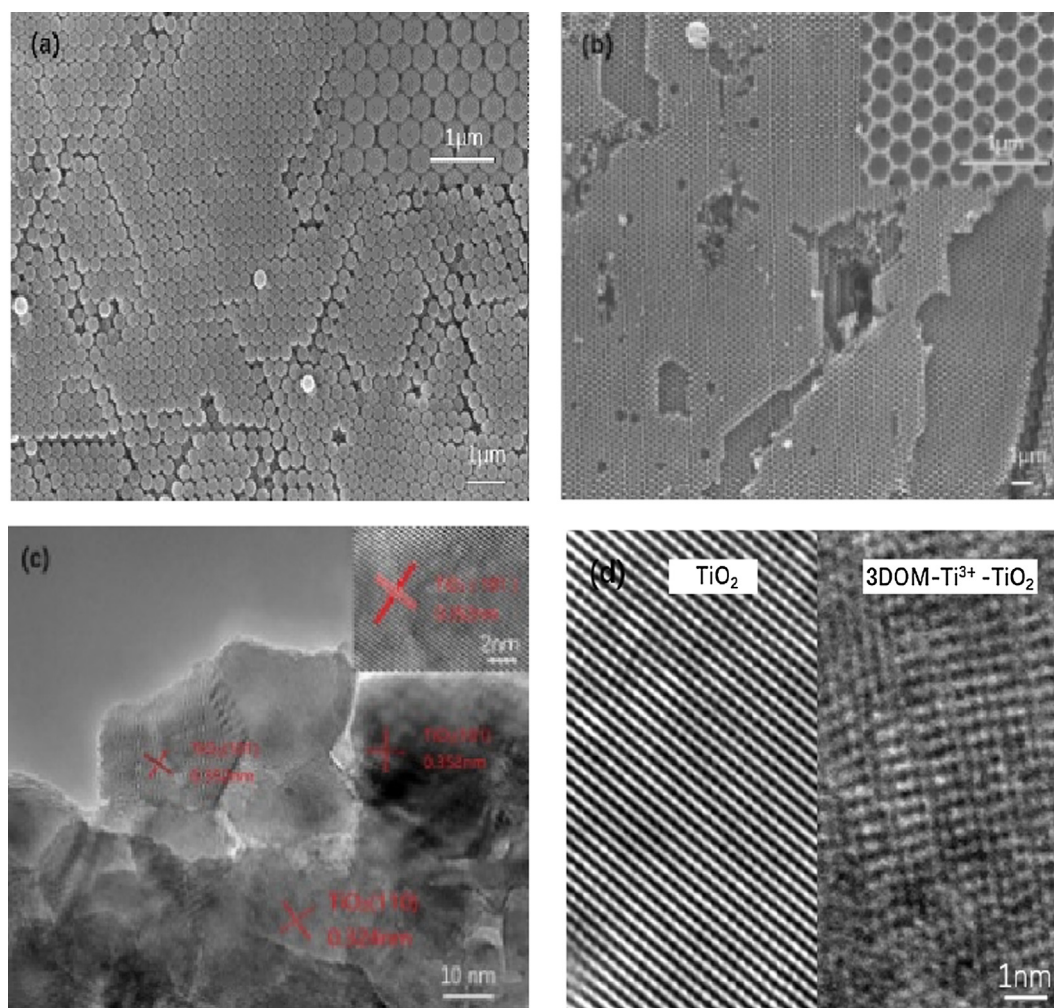


Fig. 2. SEM image of (a) PS template; (b) 3DOM-Ti<sup>3+</sup>-TiO<sub>2</sub>; TEM image of (c) 3DOM-Ti<sup>3+</sup>-TiO<sub>2</sub>; (d) TiO<sub>2</sub> (left) and 3DOM-Ti<sup>3+</sup>-TiO<sub>2</sub> (right).

temperature under a 300 W Xe lamp ( $\lambda = 420$  nm). Electrochemical impedance spectroscopy (EIS) of the samples were measured at a frequency range of 0.1 Hz to 100 kHz with a 5 mV voltage amplitude under an open-circuit voltage in a 1.0 mmol/L K<sub>3</sub>Fe(CN)<sub>6</sub> and K<sub>4</sub>Fe(CN)<sub>6</sub> solution.

### 3. Results and discussion

#### 3.1. Structure and morphology

The XRD patterns of samples are shown in Fig. 1a. All of the samples

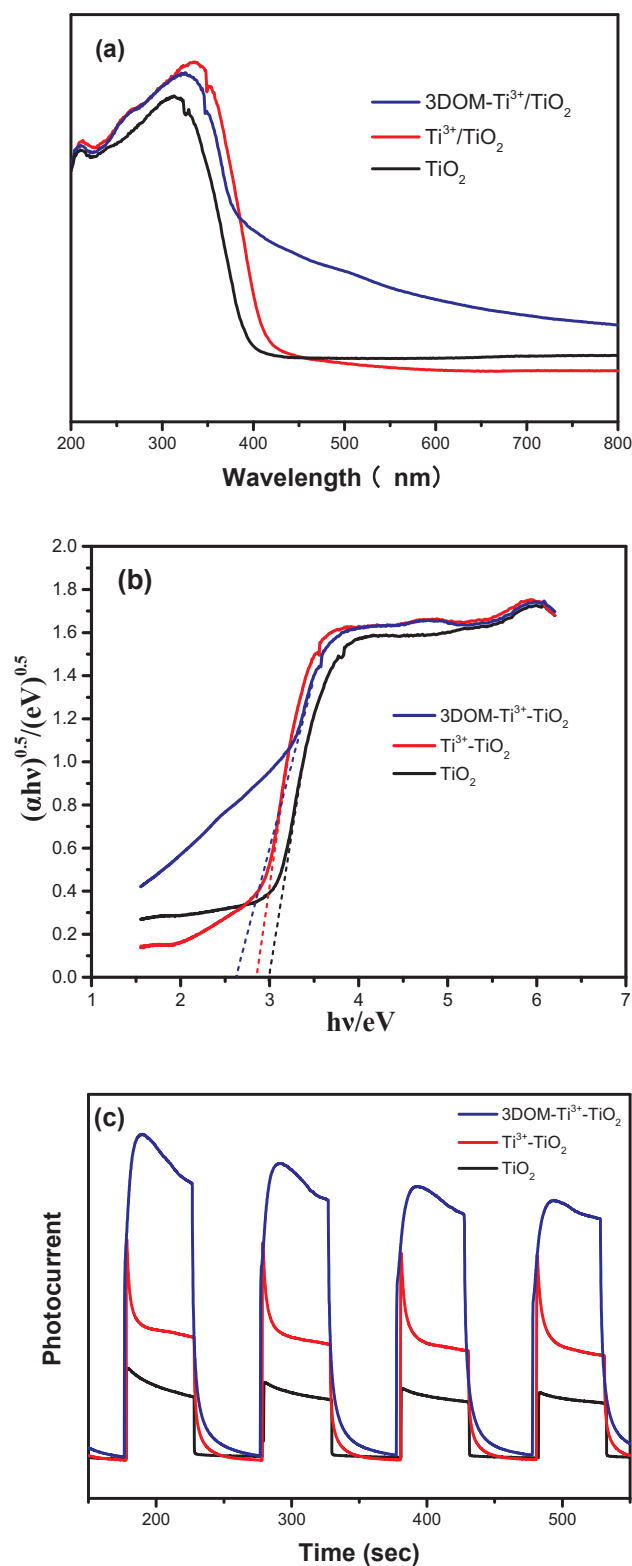


Fig. 3. UV-Vis DRS (a), Kubelka–Munk transformed reflectance spectra to estimate the optical absorption band gap (b) and Transient photocurrent densities of 3DOM-Ti<sup>3+</sup>-TiO<sub>2</sub>, Ti<sup>3+</sup>-TiO<sub>2</sub> and TiO<sub>2</sub>.

are of anatase and rutile phase and there is no obvious difference among them, indicating the less effect of PS template and ice-water quenching on the crystallinity. XPS was used to study the surface chemical composition of samples, as shown in Fig. 1b. The peaks centered at 458.7 and 464.5 eV are consistent with Ti<sup>4+</sup> in TiO<sub>2</sub> lattice at both

3DOM-Ti<sup>3+</sup>-TiO<sub>2</sub> and TiO<sub>2</sub>. However, in 3DOM-Ti<sup>3+</sup>-TiO<sub>2</sub>, there are two additional peaks centered at 457.6 (Ti2p3/2) and 463.2 eV (Ti2p1/2), which are the typical peaks of the Ti<sup>3+</sup> [17], indicating that the ice-water quenching process can create Ti<sup>3+</sup> in TiO<sub>2</sub>.

In Fig. 2a, SEM image of the PS spheres template shows it consists of numerous regularly arrayed spheres with a diameter of about 270 nm. The 3DOM-Ti<sup>3+</sup>-TiO<sub>2</sub> (Fig. 2b) shows a regularly ordered macroporous structure. Although the sample includes a part of defects, a large region of highly ordered structure hold up a main area.

As shown in Fig. 2c, the clear TEM image shows in sample 3DOM-Ti<sup>3+</sup>-TiO<sub>2</sub>, the lattice fringes spacing is 0.324 and 0.352 nm respectively, corresponding to the (1 1 0) lattice planes of rutile TiO<sub>2</sub> and (1 0 1) lattice planes of anatase TiO<sub>2</sub> respectively [18]. Besides, it can be seen from Fig. 2d that the lattice fringes of 3DOM-Ti<sup>3+</sup>-TiO<sub>2</sub> on surface are obviously distorted and tends to be disordered. It is reported that suitable lattice distortion may create more photocatalytic catalytic centers, finally resulting in an increase of photocatalytic activity [9].

### 3.2. UV-vis spectra and photoluminescence spectroscopies

Further investigations on the optical absorption property, electronic band structure, as well as photogenerated electron-hole pair recombination rate of 3DOM-Ti<sup>3+</sup>-TiO<sub>2</sub>, Ti<sup>3+</sup>-TiO<sub>2</sub> and TiO<sub>2</sub> were performed. The UV-visible absorbance spectra of samples are shown in Fig. 3a. Obviously, Ti<sup>3+</sup> self-doped TiO<sub>2</sub> displays a bigger red shift of light absorption compared with the non-doped TiO<sub>2</sub>. This result indicates that self-doping of Ti<sup>3+</sup> induced by ice-water quenching can narrow the band gap of TiO<sub>2</sub> and extend the light adsorption spectrum of TiO<sub>2</sub> to the visible-light region effectively. This could be understood as a shallow donor level is formed just below the conduction band owing to the introducing of Ti<sup>3+</sup> into TiO<sub>2</sub>, which could give rise to the band gap narrowing and visible light response of TiO<sub>2</sub> [19]. 3DOM-Ti<sup>3+</sup>-TiO<sub>2</sub> exhibits a red shift compared with Ti<sup>3+</sup>-TiO<sub>2</sub>, which should be caused by the slow photon effect of 3DOM structure materials [20,21]. Apart from that, 3DOM-Ti<sup>3+</sup>-TiO<sub>2</sub> shows a much strong visible light absorption between 400 and 800 nm. The cause is not clear, but the strong absorption in visible light region may promote the photocatalytic performance under visible light irradiation. In Fig. 3b, the estimation of band gap energies from the plots of (αhv)<sup>1/2</sup> versus the energy of absorbed light reveal shows that the band gap energies of 3DOM-Ti<sup>3+</sup>-TiO<sub>2</sub>, Ti<sup>3+</sup>-TiO<sub>2</sub> and TiO<sub>2</sub> are 2.63, 2.85 and 3.0 eV, respectively.

Fig. 3c shows a plot of photocurrent versus the irradiation time for as-prepared samples with visible light illumination. It can be seen that TiO<sub>2</sub> have a weak photocurrent response under visible light irradiation due to its wide band gap energy. For Ti<sup>3+</sup> self-doped TiO<sub>2</sub>, the photocurrent density is 1.8 times as high as TiO<sub>2</sub>. Liu et al. [9] also found that Ti<sup>3+</sup> self-doping can increase the electron transport, which is in good agreement with our results. It worth noting that the photocurrent density for 3DOM-Ti<sup>3+</sup>-TiO<sub>2</sub> is obviously higher than that of Ti<sup>3+</sup>-TiO<sub>2</sub>, demonstrating that the 3DOM structure can significantly generate more photogenerated electrons.

The N<sub>2</sub> adsorption/desorption isotherms of the synthesized samples and their corresponding pore-size distributions are shown in Fig. 4. The isotherms of TiO<sub>2</sub> and Ti<sup>3+</sup>-TiO<sub>2</sub> (Fig. 4a) are of type IV with an H<sub>2</sub> hysteresis loop (P/P<sub>0</sub> = 0.5–0.8) and characteristic of mesoporous materials, according to the IUPAC classification. The corresponding pore size distribution curve (Fig. 4b) also confirms the mesopores structure of TiO<sub>2</sub> and Ti<sup>3+</sup>-TiO<sub>2</sub>. The N<sub>2</sub> sorption isotherms of 3DOM-Ti<sup>3+</sup>-TiO<sub>2</sub> shows the characteristic type-II sorption isotherms. Moreover, the hysteresis loop was from P/P<sub>0</sub> = 0.2 to P/P<sub>0</sub> = 1.0, suggesting the existence of micropores and mesopores within macropores framework in 3DOM-Ti<sup>3+</sup>-TiO<sub>2</sub> [22]. The BET surface area for 3DOM-Ti<sup>3+</sup>-TiO<sub>2</sub> is 349.67 m<sup>2</sup>/g, which is about 3 times that of Ti<sup>3+</sup>-TiO<sub>2</sub> (112.73 m<sup>2</sup>/g) and TiO<sub>2</sub> (118.43 m<sup>2</sup>/g).

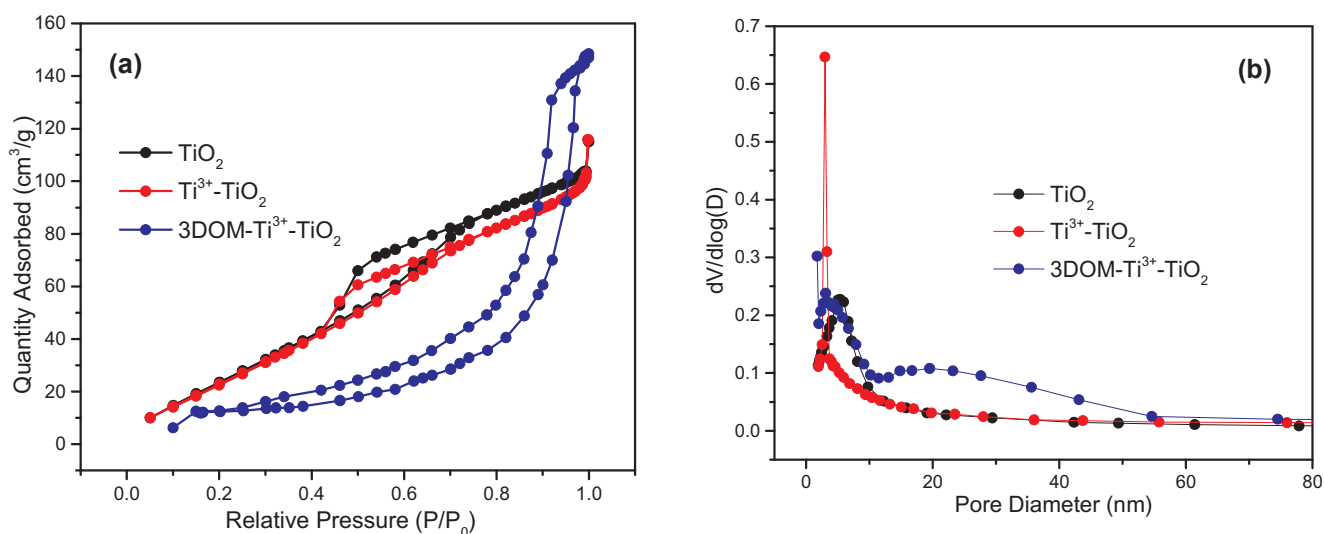


Fig. 4.  $N_2$  adsorption-desorption isotherms (a) and the corresponding pore size distribution curve (b) for the samples.

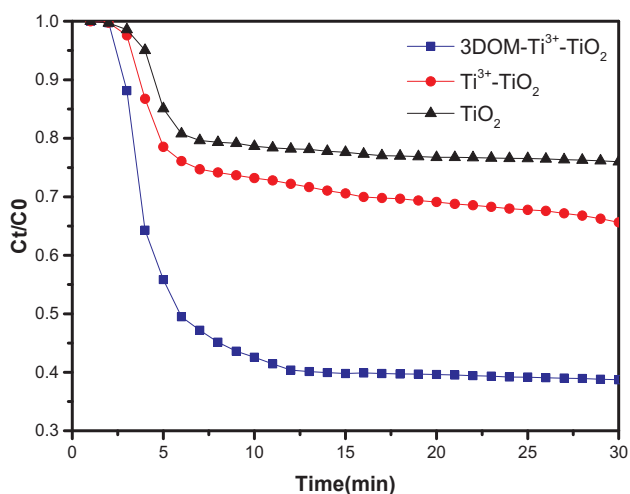
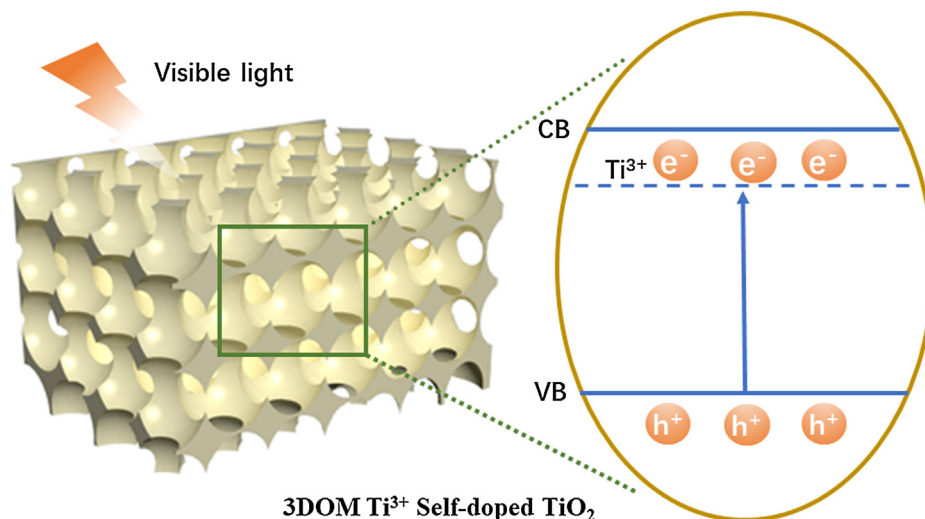


Fig. 5. Photocatalytic activity of the 3DOM- $Ti^{3+}$ - $TiO_2$ ,  $Ti^{3+}$ - $TiO_2$  and  $TiO_2$  for the removal of NO in air under visible light irradiation.

### 3.3. Photocatalytic performance

The photocatalytic performance of 3DOM- $Ti^{3+}$ - $TiO_2$ ,  $Ti^{3+}$ - $TiO_2$  and  $TiO_2$  were evaluated by their efficiencies in removing NO from continuous air flow with visible light irradiation (Fig. 5). Apparently, the  $Ti^{3+}$ - $TiO_2$  shows higher efficiency of NO removal than  $TiO_2$ , demonstrating that the  $Ti^{3+}$  doping induced by ice water quenching can promote the photocatalytic activity of  $TiO_2$ . And 3DOM- $Ti^{3+}$ - $TiO_2$  exhibits much higher photocatalytic performance compared with  $Ti^{3+}$ - $TiO_2$ , where  $\sim 60\%$  of initial nitrogen oxide was removed, suggesting that 3DOM structure can further improve the efficiency of photocatalytic removal of NO.

Therefore, according to the results, a possible photocatalytic reaction mechanism is schematic proposed in Scheme 2. Firstly, the presence of  $Ti^{3+}$  ions induced by the ice-water quenching, can make  $TiO_2$  materials visible-light responsive, which has also demonstrated by other researchers [23,24], greatly promote the efficiency of photocatalytic removal of NO under visible light irradiation. Secondly, the 3DOM structure can improve the light-harvesting efficiency [25], which is another important factor to enhance photocatalytic performance of 3DOM  $Ti^{3+}$  self-doped  $TiO_2$  for NO removal. In addition, due to the large BET surface area, it can not only adsorb more NO but also can apply more active sites, which make the excellent photocatalytic



Scheme 2. Possible photocatalytic mechanism over 3DOM  $Ti^{3+}$  self-doped  $TiO_2$ .

performance of removing NO in air for 3DOM Ti<sup>3+</sup> self-doping TiO<sub>2</sub> [26].

#### 4. Conclusions

In summary, we demonstrated for the first time the synthesis of 3DOM Ti<sup>3+</sup> self-doped TiO<sub>2</sub> with an ordered distribution of macropores in the diameter of 270 nm using a colloidal polystyrene sol-gel template and ice-water quenching method. The Ti<sup>3+</sup> self-doping and 3DOM structure with a large specific surface area act as dual-function for visible light response and efficient light harvesting in photocatalysis, which result in a higher rate of photocatalytic NO removal from continuous air flow under visible light irradiation. This manufacture technology for charge separation and light harvesting may be applied to design other excellently effective photocatalytic systems for air pollution control.

#### Declaration of interests

The authors declared that there is no conflict of interest.

#### Acknowledgements

This research was financially supported by the National Science Foundation of China (grant number 21303116) and Outstanding young academic leaders of Shanxi Provincial Department of Education (grant number 154010141-s).

#### References

- [1] J. Schneider, M. Matsuoka, M. Takeuchi, J. Zhang, Y. Horiuchi, M. Anpo, D.W. Bahnemann, *Chem. Rev.* 114 (2014) 9919.
- [2] Y. Ma, X. Wang, Y. Jia, X. Chen, H. Han, C. Li, *Chem. Rev.* 114 (2014) 9987.
- [3] Y. Li, X.Y. Wu, J. Li, K. Wang, G.K. Zhang, *Appl. Catal., B* 229 (2018) 218.
- [4] X.Y. Wu, J.T. Wang, G.K. Zhang, K. Yanagisawa, T. Sato, S. Yin, *Appl. Catal., B* 201 (2017) 128.
- [5] H. Liu, H.-T. Ma, X.-Z. Li, W.Z. Li, M. Wu, X.-H. Bao, *Chemosphere* 50 (2003) 39.
- [6] T. Ihara, M. Miyoshi, *J. Mater. Sci.* 36 (2001) 4201.
- [7] X.-X. Zou, G.-D. Li, K.-X. Wang, L. Li, J. Su, J.-S. Chen, *Chem. Commun.* 46 (2010) 2112.
- [8] B. Liu, K. Cheng, S. Nie, X. Zhao, H. Yu, J. Yu, A. Fujishima, K. Nakata, *J. Phys. Chem. C* 121 (2017) 19836.
- [9] K. Ji, H. Dai, J. Deng, H. Zang, H. Arandiyani, S. Xie, H. Yang, *Appl. Catal., B* 168 (2015) 274.
- [10] J. Jiao, Y. Wei, Y. Zhao, *Appl. Catal., B* 209 (2017) 228.
- [11] A. Stein, F. Li, R.D. Nicholas, *Chem. Mater.* 20 (2008) 649.
- [12] H. Kim, M.G. Kim, J. Cho, *Adv. Energy Mater.* 12 (2012) 1425.
- [13] Z.-X. Zhao, G.-C. Liu, B. Li, *J. Mater. Chem. A* 3 (2015) 11320.
- [14] X.-Q. Yan, C. Xue, B. Yang, G. Yang, *Appl. Surf. Sci.* 394 (2017) 248.
- [15] H. Zhao, M. Wu, J. Liu, Z. Deng, Y. Li, B.-L. Su, *Appl. Catal. B* 184 (2016) 182.
- [16] C. Dionigi, P. Nozar, D.D. Domenico, G. Calestani, *J. Colloid Interface Sci.* 275 (2004) 445.
- [17] F. Zuo, L. Wang, T. Wu, Z. Zhang, D. Borchardt, P. Feng, *J. Am. Chem. Soc.* 132 (2010) 11856.
- [18] J. Yao, Y. Zhang, Y. Wang, M. Chen, Y. Huang, J. Cao, W. Ho, S. Lee, *RSC Adv.* 7 (2017) 24683.
- [19] X. Pan, M.-Q. Yang, X. Fu, N. Zhang, Y.-J. Xu, *Nanoscale* 5 (2013) 3601.
- [20] Q. Zhou, L. Li, Y. Xin, D. Liu, X. Zhang, *New J. Chem.* 42 (2018) 15190.
- [21] Y. Wei, J. Jiao, Z. Zhao, W. Zhong, J. Li, J. Liu, G. Jiang, A. Duan, *J. Mater. Chem. A* 3 (2015) 11074.
- [22] G. Zhai, J. Wang, Z. Chen, S. Yang, Y. Men, *J. Hazard. Mater.* 363 (2019) 214.
- [23] X. Chen, L. Liu, P.-Y. Yu, S.-S. Mao, *Science* 331 (2011) 746.
- [24] X. Chen, L. Liu, F. Huang, *Chem. Soc. Rev.* (2015) 1861.
- [25] J. Liu, Y. Li, H.-W. Huang, C. Wang, M. Wu, L.-H. Chen, B.-L. Su, *J. Mater. Chem. A* 2 (2014) 5051.
- [26] H.Y. Zhu, R. Jiang, Y.Q. Fu, R.R. Li, J. Yao, S.T. Jiang, *Appl. Surf. Sci.* 369 (2016) 1.